Numerical simulation of an evaporative meniscus on a moving substrate

Frédéric Doumenc, Béatrice Guerrier

EPJ manuscript No.
(will be inserted by the editor)

Numerical simulation of an evaporative meniscus on a moving substrate

Frédéric Doumenc[1,a] and Béatrice Guerrier[1]

UPMC Univ Paris 06, Univ Paris-Sud, CNRS, UMR 7608, Lab. FAST, Bât 502, Campus Universitaire, Orsay, F-91405, France

Abstract. A hydrodynamic model based on lubrication theory has been developed to describe an evaporative meniscus in a complete wetting configuration, when evaporation takes place in ambient air. We focus on combined effects of evaporation and the substrate motion on the effective contact angle. Numerical simulations show two distinct regimes when varying the substrate velocity on several orders of magnitude. At a small velocity, the effective contact angle is governed by evaporation and is independent of the substrate velocity, while the substrate motion is dominant at a high velocity. In the latter case, a Landau-Levich regime is obtained for the receding contact line, and a Cox-Voinov regime for the advancing contact line. Finally, we use our numerical results to test the simplified model developed by Pham *et al.* [5,6].

1 Introduction

Evaporation close to a contact line can modify the effective contact angle observed at the macroscopic scale [1, 2]. If, in addition, there is a relative motion between the substrate and the contact line, the effective contact angle dynamically depends on both evaporative flux and the substrate velocity. In this work, we focus on the case of complete wetting of pure liquids with evaporation in an inert gas.

The case of droplets has been experimentally studied by A. M. Cazabat's group [3,4]. The droplet spreads over the substrate until it reaches a maximum diameter. Then, due to evaporation, the droplet retracts, until it completely vanishes. These authors obtained from experiments simple power laws describing the time evolution of the contact angle and the droplet radius during the receding stage. Unlike in droplets, a steady state regime can be reached in dip-coating like experiments. This is the configuration considered in this work.

When evaporation takes place in ambient air, the evaporative flux is limited by vapor diffusion in the gas phase. Close to the contact line, the liquid and gas phases are coupled through the Kelvin effect. Poulard *et al.* [3] and Pham *et al.* ([5] with erratum [6]) proposed approximate models based on the Deegan's electrostatic analogy [7] to estimate *a priori* the profile of the evaporative flux. Although using different ways to overcome the unphysical divergence of the Deegan's expression at the contact line, all of these authors found the same scaling for the precursor film length, as well as the effective contact angle, in the case of a motionless substrate. Recently, Eggers and Pismen [8] developed a more elaborate model taking explicitly into account the coupling between the liquid and gas phases, in the case of retracting droplets, and they found a good agreement with Cazabat's experiments. In a previous work, we developed the same type of approach for a meniscus between two parallel plates (capillary rise)[9]. Scaling laws describing the different domains of the meniscus have been derived in the steady state and for a motionless substrate, and validated by numerical simulations. Despite the different descriptions of the tip, the scalings of the precursor film length and the contact angle were found to be the same as those predicted by the above-mentioned approximate models [3,5]. This new study focuses on the combined effects of evaporation and the substrate motion.

2 Model description

The model described herein has first been developed for polymer solutions [10], then it has been modified to address the problem of pure liquids on a motionless substrate [9]. We present in the following the extension of the latter case to a moving substrate. The process is assumed isothermal (same temperature T in liquid and gas

[a] e-mail: frederic.doumenc@upmc.fr

phases, equal to the ambient temperature). The Stokes equations in the liquid phase are written in the framework of lubrication approximation, with a disjoining pressure approach to describe van der Waals interactions between the liquid and the solid substrate. The volumetric flow rate $Q(x)$ over a cross section at abscissa x along the substrate reads [11]:

$$Q(x) = \int_0^{h(x)} u(x,z)dz = \frac{h^3}{3\eta}\frac{\partial}{\partial x}(\sigma\frac{\partial^2 h}{\partial x^2} + \frac{A}{6\pi h^3}) + Vh \tag{1}$$

where $u(x,z)$ is the velocity component in the direction parallel to the substrate, z the distance to the substrate, h the liquid height, η the dynamic viscosity, σ the surface tension, A the Hamaker constant and V the substrate velocity. In the steady state, the global mass conservation reads:

$$\frac{\partial Q}{\partial x} = -v_{ev}(x) \tag{2}$$

where $v_{ev}(x)$ is the local evaporation velocity (positive for evaporation). At $x = 0$, we impose the liquid height $h(0) = h_0$ and the curvature $h_{xx}(0) = C_0$. These boundary conditions create a meniscus of length of the order of $L_{st} = \sqrt{2h_0/C_0}$. A second set of two boundary conditions is imposed at $x = W$ ($W > L_{st}$). The first condition consists in zero curvature ($h_{xx}(W) = 0$), while the second one depends on the direction of the substrate motion: a receding contact line ($V > 0$), or an advancing contact line ($V < 0$). A zero slope condition is assumed in the former case ($h_x(W) = 0$), while an arbitrary small thickness is imposed in the latter case ($h(W) = h_{end}$ with $h_{end} \sim 1\text{nm}$). As far as the length W of the simulation box is large enough, the choice of the conditions at $x = W$ (including the value of the height h_{end}) has no significant effect on the results.

As evaporation takes place in air, it is driven by vapor transport in the gas phase. So the coupling between liquid and gas must be explicitly taken into account, making the determination of the evaporative flux a non-local problem [8]. The gas domain is assumed to be rectangular of length W and height H ($H \gg h_0$, so variations of the liquid height can be neglected in the gas phase model). Assuming a stagnant air and a dilute vapor, the vapor concentration in the gas phase c_g is computed by solving the diffusion equation:

$$\frac{\partial^2 c_g}{\partial x^2} + \frac{\partial^2 c_g}{\partial z^2} = 0 \qquad \text{for } 0 < x < W \text{ and } 0 < z < H. \tag{3}$$

The lateral boundaries are assumed impermeable. The coupling with the liquid phase is obtained by writing the local thermodynamic equilibrium and the mass flux conservation at the free surface for $0 \leq x \leq W$ and $z = 0$:

$$c_g = c_{gs0}\, exp[-\frac{\bar{v}_s}{RT}(\sigma\frac{\partial^2 h}{\partial x^2} + \frac{A}{6\pi h^3})] \qquad \text{and} \qquad \rho\, v_{ev} = -D_g\frac{\partial c_g}{\partial z} \tag{4}$$

where R is the ideal gas constant, $\bar{v}_s$ is the liquid molar volume, ρ is the liquid density, D_g is the vapor diffusion coefficient in the gas phase, and $c_{gs0} = M_s P_{vs0}(T)/(RT)$ is the vapor concentration at the bulk saturated vapor pressure $P_{vs0}(T)$ (M_s is the solvent molar mass). Finally, a known vapor concentration c_{gH} deduced from the ambient solvent activity $a_\infty = c_{gH}/c_{gs0}$ is imposed at $z = H$. In a previous work [9], we showed that the average evaporation velocity $\bar{v}_{ev}$ at the meniscus free surface depends on the system properties and geometric parameters through the following scaling:

$$\bar{v}_{ev} \sim v_{ev}^{sc} \equiv \frac{D_g}{\rho H}(c_{gs0} - c_{gH})\frac{W}{L_{st}} \tag{5}$$

Equations (1) - (4) with the above-defined boundary conditions are solved by finite differences, with an adaptive mesh algorithm to increase the number of nodes in the region of a high evaporation rate (see [9] for details). We carefully checked over several test cases that the results were independent of the numerical parameters.

We used this model to simulate evaporation of toluene in air at the atmospheric pressure (see [9] for physical properties). The temperature is $T = 25°C$. The geometric parameters are $h_0 = 0.1$ mm, $C_0 = 2$ mm^{-1}, $W = 1$ mm, $H = 3$ mm. We consider two values of the Hamaker constant ($A = 10^{-20}$ J and $A = 10^{-19}$ J), and two values of the ambient solvent activity ($a_\infty = 0$ and $a_\infty = 0.5$, corresponding to $v_{ev}^{sc} = 1.4$ μm.s^{-1} and $v_{ev}^{sc} = 0.71$ μm.s^{-1}, respectively).

3 Advancing contact line

Figure 1 shows some typical results in the case of an advancing contact line, for the film thickness, the curvature, the liquid pressure and the evaporative flux as a function of the horizontal distance x, for several capillary numbers $Ca \equiv \eta V/\sigma$. Two regimes can be observed, depending on the value of Ca. For small capillary numbers ($|Ca| \lesssim 2 \times 10^{-6}$), the meniscus shape is independent of Ca, and the departure from the thermodynamic equilibrium

(corresponding to $Ca = 0$ and $v_{ev} = 0$) is due to evaporation only. On the contrary, the meniscus shape is significantly modified by the substrate motion for $|Ca| \gtrsim 2 \times 10^{-6}$. As pointed out in [9], it is an advantage of this type of model to predict the meniscus structure, from the quasi-static region characterized by a quasi-constant curvature C_0 and a quasi-constant pressure $\sigma C_0 = 60$ Pa, to the liquid film adsorbed on the substrate and governed by the disjoining pressure. The peaks of the evaporation velocities in Fig. 1d are due to the bidimensional nature of vapor transfer in the gas phase, like in Deegan's approach, but there is no divergence there due to the Kelvin effect (see Fig. 1c along with Eq. (4)). At the highest capillary number ($|Ca| = 1.8 \times 10^{-4}$, corresponding to $|V| = 1$ cm.s^{-1}), a small region of condensation (negative evaporation rate) is detected just after the peak.

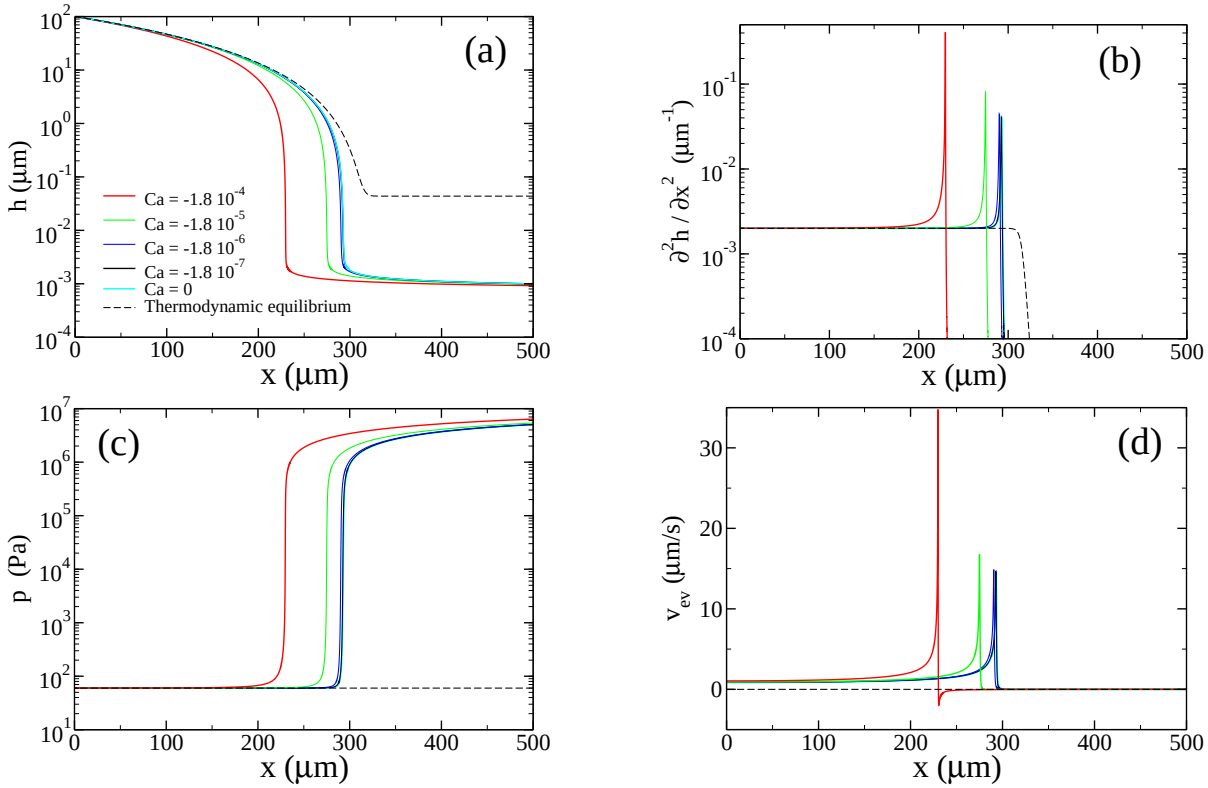

Fig. 1. Advancing contact line for $a_\infty = 0$ and $A = 10^{-19}$ J (increasing $|Ca|$ from right to left). (a): the liquid thickness ; (b): the curvature ; (c): the pressure $p = \sigma \frac{\partial^2 h}{\partial x^2} + \frac{A}{6\pi h^3}$; (d): the evaporation velocity.

A precise definition of the contact angle is not straightforward. Indeed, strictly speaking, such angle does not exist, since there is no intersection between the liquid profile and the substrate (see Fig. 1a). Nevertheless, an effective (or apparent) contact angle can still be defined to describe the shape of the meniscus at the macroscopic scale. This requires a more detailed description of the quasi-static region. This region extends from $x = 0$ to $x = x_1$, with x_1 the abscissa corresponding to a significant deviation of the pressure p from the static capillary pressure: $(p(x_1) - \sigma C_0)/\sigma C_0 < \alpha$ (α an arbitrary parameter, $0 < \alpha < 1$). Due to the fact that the curvature can be regarded as constant in that region, and within the framework of small slope approximation, the liquid height is given by a parabolic function: $h_{qs}(x) = h_0 + S_0 x + C_0 x^2/2$. S_0 is the slope at $x = 0$, which can be easily deduced from numerical simulations. After extrapolation, this parabola intercepts the substrate at abscissa x_2 such that $h_{qs}(x_2) = 0$. We can consider two definitions of the effective contact angle:

$$\theta_1 = \frac{\partial h}{\partial x}(x_1) \quad \text{and} \quad \theta_2 = \frac{\partial h_{qs}}{\partial x}(x_2) = S_0 + C_0 x_2. \tag{6}$$

θ_1 is the slope at the transition between the quasi-static and the dynamic region, while θ_2 is the slope of the parabola describing the quasi-static region at the intersection with the substrate.

Figure 2 shows θ_1 and θ_2 as a function of the capillary number Ca, for different values of A and a_∞. Both definitions lead to the same qualitative results. At a low substrate velocity, the contact angle is independent of the capillary number, as expected. On the contrary, at a high velocity, a classical Cox-Voinov regime is found, in which $\theta \propto Ca^{1/3}$. In this high velocity regime, we expect evaporation to have a weak effect on the meniscus macroscopic behavior.

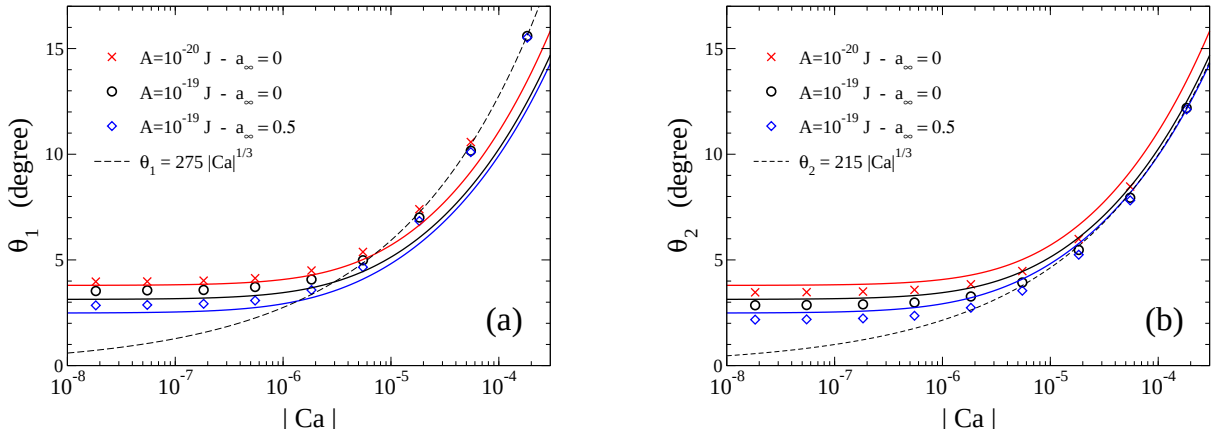

Fig. 2. Effective contact angle as a function of the capillary number for an advancing contact line. Symbols: numerical simulations ; solid lines: Eq. (7) ; dashed lines: fit of the Cox-Voinov regime. (a): θ_1 for $\alpha = 0.1$; (b): θ_2.

Switching from θ_1 to θ_2 yields a decrease in the estimation of the contact angle by approximately 20%. We can also estimate the effect on θ_1 of the arbitrary parameter α which has been set to 0.1 in Fig.2a. Taking $\alpha = 0.03$ or $\alpha = 0.3$ leads to variations of the same order, between 10 and 30%. This uncertainty is inherent to the definition of the effective contact angle. The same problem is encountered in experiments. Indeed, Guéna *et al.* [4] measured by interferometry the effective contact angle of evaporating droplets at the contact line or at the inflection point of the droplet profile, and found differences of the same order as above between the two estimates.

In the following, we use these simulation results to test the approximate model proposed by Pham *et al.* ([5, 6]. They use the Deegan's electrostatic analogy [7] to obtain an estimate of the evaporation flux. For small contact angles, and assuming that the contact line is located at $X = 0$, the volumetric evaporative flux reads: $J(X) = J_0/\sqrt{X}$. A small arbitrary liquid height and a zero slope are imposed at $X = 0$. A zero curvature is imposed at a macroscopic distance L_{macro} from the contact line. This leads to the following analytical expression for the effective contact angle:

$$\theta^3 = 3.17\ \theta_m^3 - 9\ Ca\ (\ln \frac{L_{macro}}{l_{micro}} + 1) \tag{7}$$

with $\theta_m = 2.12 \frac{J_0^{1/3}\eta^{1/3}}{A^{1/12}\sigma^{1/4}}$ being the angle at the small scale cut-off $l_{micro} = 3.4(\frac{A}{12\pi J_0 \eta})^{2/3}$ (cf. [5,6] for details). We choose $L_{macro} = L_{st}$ as an estimation of the macroscopic scale. This is certainly an overestimation, but the ratio L_{macro}/l_{micro} has only a weak effect on the results, since it is included in a logarithm. The constant J_0 is estimated from the mean evaporation velocity: $J_0 = v_{ev}^{sc}\sqrt{L_{st}}/2$. Figure 2a and 2b show a good agreement between the approximate model and the numerical simulations. Indeed, the differences are of the same order as the uncertainty coming from the definition of the contact angle.

4 Receding contact line

A similar behavior is observed in the case of a receding contact line (see Fig. 3), that is a regime dominated by the plate motion at small Ca ($Ca \gtrsim 6 \times 10^{-6}$) and by evaporation at even smaller Ca ($Ca \lesssim 6 \times 10^{-6}$). The former case corresponds to the Landau-Levich regime in which friction induced by the plate movement is high enough to pull out a liquid film which evaporates over a distance increasing with the plate velocity (see the experimental study by Qu *et al.* [12]). At the highest capillary number ($Ca = 1.8 \times 10^{-5}$, corresponding to $V = 1$ mm/s), the distance required to achieve complete evaporation of the liquid film is higher than the domain width W. In that case, the liquid film inside the computational domain is too thick to activate the Kelvin effect, so the concentration field in the gas phase is one-dimensional, and the evaporation velocity represented in Fig. 3b is uniform.

The effective contact angle θ_1 being too sensitive to α close to the transition from the evaporative to the Landau-Levich regimes, we only present results for θ_2 (see Fig. 4). θ_2 is independent of Ca in the evaporative regime, then falls down to zero at the transition with the Landau-Levich regime. Once again, the model by Pham *et al.* (Eq. 7) gives fairly good results, as compared to the numerical simulations. It is interesting to notice that the order of magnitude of the capillary number corresponding to the transition between the two regimes can be estimated by setting $\theta = 0$ in Eq. 7.

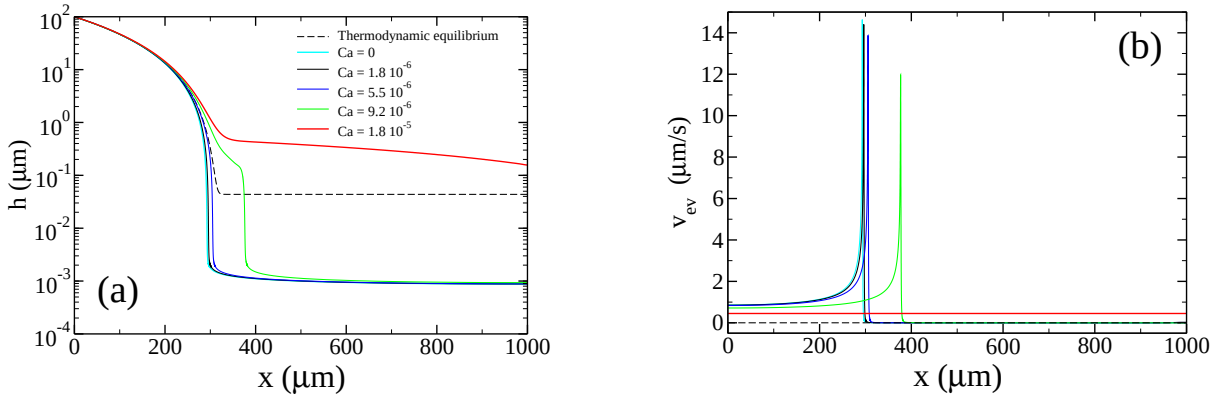

Fig. 3. Receding contact line for $a_\infty = 0$ and $A = 10^{-19}$ J. (a): the liquid thickness (increasing Ca from left to right) ; (b): the evaporation velocity.

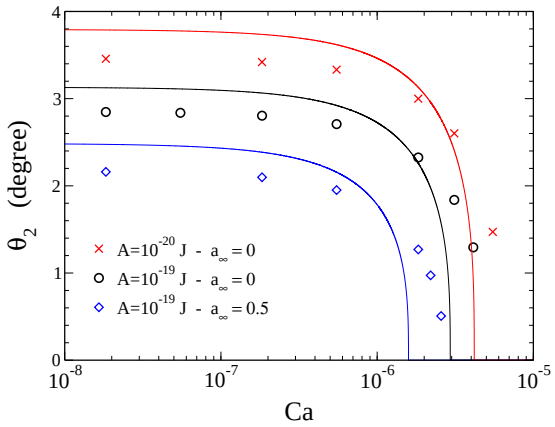

Fig. 4. Effective contact angle as a function of the capillary number Ca for a receding contact line. Symbols: numerical simulations; solid lines: Eq. (7).

5 Conclusion

We proposed a hydrodynamic model based on lubrication theory to describe an evaporative meniscus in a complete wetting configuration, when evaporation takes place in ambient air. van der Waals interactions were taken into account *via* a disjoining pressure term. We focused on combined effects of evaporation and the substrate motion on the effective contact angle. Numerical simulations showed two distinct regimes when varying the capillary number over several orders of magnitude. At a very small capillary number, the effective contact angle is governed by evaporation and is independent of the substrate velocity. On the contrary, the substrate motion is dominant at a high velocity: the Cox-Voinov regime is obtained in the case of an advancing contact line, and the Landau-Levich regime in the case of a receding contact line. Finally, our numerical results were used to test the simplified model developed by Pham *et al.* [5,6]. This model shows a good agreement with our results within the range of uncertainty inherent to the definition of the effective contact angle.

References

1. Wayner P.C., *Langmuir* **9**, pp. 294-299, 1993.
2. Bourgès-Monnier C., Shanahan M.E.R., *Langmuir* **11**, pp. 2820-2829, 1995.
3. Poulard C., Guéna G., Cazabat A.M., Boudaoud A., Ben Amar M., *Langmuir* **21**, pp. 8226-8233, 2005.
4. Guéna G., Allençon P., Cazabat A.M., *Coll. Surf.* **300**, pp. 307-314, 2007.
5. Pham C.T., Berteloot G., Lequeux F. and Limat L., *Europhys. Lett.* **92**, 54005, 2010.
6. Pham C.T., Berteloot G., Lequeux F. and Limat L., *Europhys. Lett.* **93**, 69901, 2011.
7. Deegan R.D., Bakajin O., Dupont T.F., Huber G., Nagel S.R. and Witten T.A, *Phys Rev. E* **62**, pp.756-765, 2000.
8. Eggers J., Pismen L.M., *Phys. Fluids* **22**, 112101, 2010.
9. Doumenc F., Guerrier B., *Eur. Phys. J. Special Topics* **197**, pp. 281-293, 2011.

10. Doumenc F., Guerrier B., *Langmuir* **26**, pp. 13959-13967, 2010.
11. Oron A., Davis S.H., Bankoff S.G., *Rev. Mod. Phys.* **69**, pp. 931-980, 1997.
12. Qu D., Ramé E. and Garoff S., *Phys. fluids* **14**, pp. 1154-1165, 2002.